This is an open access article published under a Creative Commons Non-Commercial No Derivative Works (CC-BY-NC-ND) Attribution License, which permits copying and redistribution of the article, and creation of adaptations, all for non-commercial purposes.

ACS AUTHORCHOICE

JACS
JOURNAL OF THE AMERICAN CHEMICAL SOCIETY

pubs.acs.org/JACS

Article

Enhancing Long-Range Energy Transport in Supramolecular Architectures by Tailoring Coherence Properties

Bernd Wittmann, Felix A. Wenzel, Stephan Wiesneth, Andreas T. Haedler, Markus Drechsler, Klaus Kreger, Jürgen Köhler, E. W. Meijer, Hans-Werner Schmidt,* and Richard Hildner*

Cite This: J. Am. Chem. Soc. 2020, 142, 8323−8330

Read Online

ACCESS | Metrics & More | Article Recommendations | Supporting Information

ABSTRACT: Efficient long-range energy transport along supramolecular architectures of functional organic molecules is a key step in nature for converting sunlight into a useful form of energy. Understanding and manipulating these transport processes on a molecular and supramolecular scale is a long-standing goal. However, the realization of a well-defined system that allows for tuning morphology and electronic properties as well as for resolution of transport in space and time is challenging. Here we show how the excited-state energy landscape and thus the coherence characteristics of electronic excitations can be modified by the hierarchical level of H-type supramolecular architectures. We visualize, at room temperature, long-range incoherent transport of delocalized singlet excitons on pico- to nanosecond time scales in single supramolecular nanofibers and bundles of nanofibers. Increasing the degree of coherence, i.e., exciton delocalization, via supramolecular architectures enhances exciton diffusivities up to 1 order of magnitude. In particular, we find that single supramolecular nanofibers exhibit the highest diffusivities reported for H-aggregates so far.

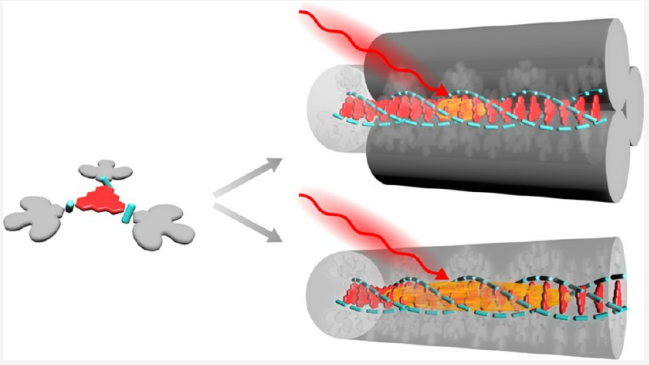

INTRODUCTION

Supramolecular chemistry provides intriguing opportunities to create nano- to mesoscale assemblies with unprecedented optical and electronic functionalities owing to cooperative interactions between the constituent building blocks.[1−7] A key functionality for potential applications is, for example, efficient long-range excitation energy transport.[4,8−14] In general, energy transport in organic materials is governed by the delicate interplay between electronic Coulomb coupling between densely packed molecules and electronic and structural disorder. On the one hand, electronic coupling leads to the formation of delocalized exciton states; that is, electronic excitations are coherently shared by many molecules, which we refer to as (quantum) coherent transport. On the other hand, electronic and structural disorder leads to a localization of excitons on small domains of supramolecular assemblies.[15,16] If disorder dominates, long-range transport cannot be realized, because incoherent Förster-type hopping of strongly localized excitons limits transport to some tens of nanometers.[17] In contrast, reducing disorder increases exciton delocalization, and thus the degree of coherence.[15,18−20] Such combined incoherent−coherent transport, i.e., incoherent hops of delocalized excitons,[12,21−24] with a strong contribution of coherence, indeed allowed achieving distances beyond 1 μm.[12,23] However, a full understanding and control of long-range energy transport is still highly complex, because in supramolecular nanostructures the electronic coupling and disorder are typically of the same order of magnitude. This so-called intermediate regime renders disentangling the different contributions to energy transport difficult, on both the theoretical and experimental side.[16] Since transport efficiencies and distances are predicted to be largest in this regime,[21,25,26] a unique picture is desirable for the design of novel excitonic materials and devices.[2,4,5,7−9]

A straightforward approach to modify electronic coupling and disorder makes use of the self-assembly of defined nanostructures based on the same building blocks. In this context, so-called pathway complexity can be exploited to form thermodynamically and kinetically stable supramolecular aggregates with different structural order[6,27,28] and thus with significantly altered photophysical and energy transport properties. In contrast, supramolecular aggregates with different hierarchical levels[11,29−31] feature the same structural arrangement of the building blocks, i.e., the same electronic coupling, with only subtle variations in the local electronic

Received: February 7, 2020
Published: April 11, 2020

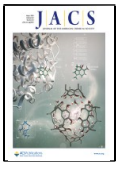

Downloaded via UNIV BAYREUTH on May 13, 2020 at 11:49:14 (UTC).
See https://pubs.acs.org/sharingguidelines for options on how to legitimately share published articles.

© 2020 American Chemical Society

https://dx.doi.org/10.1021/jacs.0c01392
J. Am. Chem. Soc. 2020, 142, 8323−8330

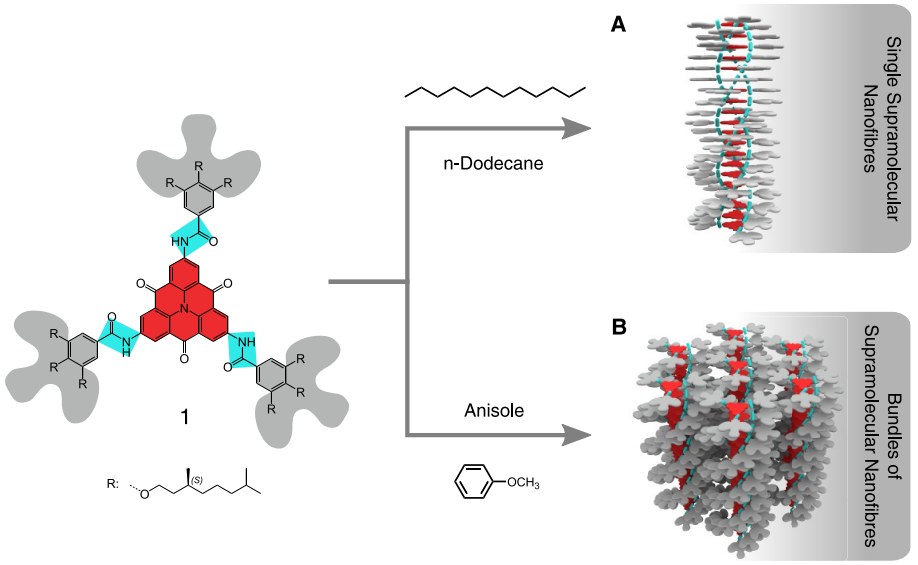

Figure 1. Supramolecular architectures of compound **1** with different hierarchical levels. Left: Compound **1** comprising a carbonyl-bridged triarylamine core (red), three amide moieties (blue), and chiral bulky peripheries (gray). Self-assembly in *n*-dodecane results in single supramolecular nanofibers (A) and in anisole in bundles of supramolecular nanofibers (B).

environment. Such structures are therefore ideal candidates to reveal the interplay between the electronic coupling and disorder.

Here we present stable and robust supramolecular architectures based on a carbonyl-bridged triarylamine trisamide (CBT, compound **1**, see ref 32) with different hierarchical levels depending on the solvent, i.e., single supramolecular nanofibers and bundles of supramolecular nanofibers (Figure 1). The molecular design of compound **1** results in columnar structures with a well-defined, cofacial H-type arrangement of the CBT cores that is driven by directed hydrogen bonding between amide groups. Excitons in these supramolecular architectures possess different degrees of coherence (delocalization), tuned by bundling-induced electronic disorder. We are thus able to resolve the competition between coherence and disorder and to demonstrate its impact on long-range, pico- to nanosecond, incoherent transport of singlet excitons in supramolecular architectures on the level of single nanostructures at room temperature. In contrast to previous work on nanotubular assemblies,[11,30] we find a higher degree of coherence and thus enhanced exciton diffusivities in single supramolecular nanofibers.

RESULTS AND DISCUSSION

Controlled Self-Assembly of Single Nanofibers and Bundles of Nanofibers. Using two selected solvents, we are able to self-assemble compound **1** into distinct supramolecular morphologies (see Supporting Information section 1). In *n*-dodecane, compound **1** forms single supramolecular nanofibers of several micrometers in length (Figures 2A and S1) and uniform heights of about 2 nm (Figure 2B), as shown by atomic force microscopy (AFM), which is consistent with our previous work on single CBT-nanofibers.[23,32] Transmission electron microscopy (TEM, Figure 2C) reveals single supramolecular nanofibers and nanofibers partially located next to each other due to sample preparation. The selected area electron diffraction (SAED) pattern features a signal corresponding to a distance of 0.33 nm (Figure 2D) caused by cofacial stacking of CBT cores along the supramolecular nanofibers.[23,32]

Self-assembly of compound **1** in anisole results in bundles of supramolecular nanofibers with widths and heights on the order of 100 nm, as shown by AFM and TEM measurements (Figure 2E,F,G and Figure S1). The SAED pattern yields the characteristic cofacial stacking distance of 0.33 nm between CBT cores (Figure 2H). Additionally, SAED at smaller angles (Figure S2) reveals defined signals corresponding to a distance of 2.8 nm. Assuming a columnar hexagonal packing of the nanofibers,[32] we obtain an intercolumnar spacing of 3.2 nm. This distance is substantially smaller than the calculated diameter of about 4.4 nm for the extended compound **1**.[32] In bundles the peripheries of adjacent nanofibers therefore strongly interact. Based on these data, we estimate that one bundle consists of approximately 2000 nanofibers.

Optical Properties of Nanofibers and Bundles. UV–vis and photoluminescence (PL) spectra of dissolved compound **1** in THF (Figure 3A) exhibit the characteristic vibronic progression of an aromatic molecule (see Supporting Information section 4, Table S1). The maxima at 460 nm and 490 nm, respectively, are attributed to the electronic (0–0) $\pi-\pi^*$ transition of the CBT core.[33,34]

The absorption spectra of supramolecular nanofibers and bundles of nanofibers are shown in Figure 3B and C, respectively (see also Figure S3). Both feature a substantially reduced intensity of the highest-wavelength (lowest-energy) peak around 520 nm (labeled A_1) compared to the spectrum of dissolved compound **1**. This spectral change is characteristic for delocalized absorbing excitons in H-aggregates, formed by substantial electronic Coulomb coupling between adjacent CBT cores.[35] Circular-dichroism spectra of dispersions of both supramolecular morphologies feature nearly identical signatures (Figure S4) indicating no significant difference in the structural arrangement of the CBT cores in supramolecular nanofibers and bundles of nanofibers.

After absorption rapid, subpicosecond relaxation within the exciton bands takes place toward lower-energy, relaxed exciton states,[22] from where emission occurs (see Supporting

https://dx.doi.org/10.1021/jacs.0c01392
J. Am. Chem. Soc. 2020, 142, 8323–8330

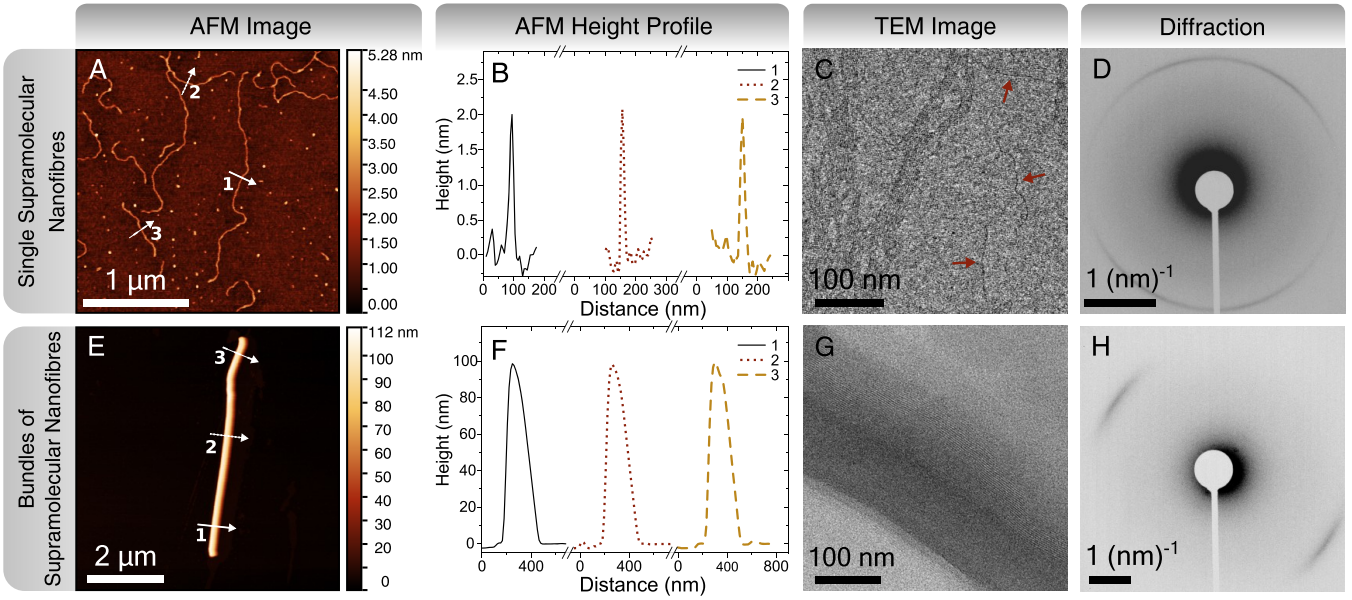

Figure 2. Morphological and structural characterization of the supramolecular architectures. (A) AFM image (topographical scan) of single supramolecular nanofibers prepared from a dispersion of compound **1** in *n*-dodecane (4 μM, ~10 ppm). (B) Height profiles along the arrows labeled in A. (C) TEM image of single nanofibers partially located next to each other (40 μM, ~100 ppm). Arrows indicate isolated single nanofibers. (D) SAED pattern corresponds to a stacking distance of 0.33 nm between CBT cores. (E) AFM image of a bundle of supramolecular nanofibers prepared from a dispersion of compound **1** in anisole (40 μM, ~100 ppm). (F) Height profiles along the arrows labeled in E. (G) TEM image of a bundle of nanofibers. (H) SAED pattern corresponds to a stacking distance of 0.33 nm.

Information section 4, Figure S5). In the PL spectrum of supramolecular nanofibers the 0−0 peak seems to be absent at room temperature (Figure 3B, see also Supporting Information section 4, Figure S6). These data suggest a large degree of electronic order and thus of coherence with a pronounced delocalization of relaxed emitting excitons[35] along nanofibers. In contrast, the corrected PL spectrum of bundles of nanofibers (Figures 3C and S7) features a 0−0 peak that is only slightly suppressed compared to that of dissolved compound **1**. This observation indicates strong localization of the relaxed emitting exciton over only a few CBT cores and thus a small degree of coherence. The localization must result predominantly from electronic disorder, because the structural order within the columns of both architectures appears to be comparable (Figure S4). Our data for bundles of nanofibers thus demonstrate a rapid disorder-induced localization of initially delocalized absorbing excitons prior to emission.[21]

The influence of electronic disorder on the relaxed emitting excitons in our supramolecular architectures is further confirmed by the trend in the excited-state lifetimes (PL quantum yields), which increase (decrease) from 2.7 ns (13.8%) for the dissolved compound **1** to 3.5 ns (2.6%) for bundles and 5.4 ns (1.3%) for single nanofibers (see Table S2 and Figure S8). This enhancement in lifetimes is highly beneficial for long-range energy transport,[15] as we previously reported.[23]

To quantify the electronic Coulomb coupling and the electronic disorder between CBT cores from the spectra in Figure 3B,C, we performed numerical simulations based on the theory of Spano and co-workers using a disordered Holstein Hamiltonian (ref 35 and Supporting Information section 5). The intercolumnar distance of 3.2 nm within bundles prevents delocalization of electronic excitations between columns. A bundle is thus modeled as an arrangement of independent nanofibers. Electronic (energy) disorder is included by taking the CBT cores' transition energy offsets from a Gaussian distribution with a width σ. Moreover, we include a correlation length l_0 that accounts for differences in the spatial distribution of disorder in the transition energies (Figure S5).

The simulations (Figure 3B,C, black lines) agree very well with the experimental data in the relevant spectral region. The absorption spectra of both architectures are well described by a common set of parameters, i.e., by an electronic coupling of J_0 = 735 cm^{-1} (91 meV) and an electronic disorder of σ = 1036 cm^{-1} (130 meV, see Figure S9 and Supporting Information section 5), which places both morphologies in the intermediate coupling regime.

The differences between the PL spectra of nanofibers and bundles can only be modeled using different correlation lengths. The absence of the 0−0 PL peak in the spectrum of nanofibers requires a correlation length of $l_0 \geq 10$ CBT cores with a disorder of σ = 1076 cm^{-1} (134 meV, see Supporting Information section 5). Due to this spatial correlation in the transition energies, a nanofiber is segmented into domains that possess a rather uniform excited-state energy landscape (Figure 3E). The delocalization of the relaxed, emitting singlet excitons can then be quantified by the coherence number of $N_{coh} \geq 5.4$ CBT cores. In contrast, the strong 0−0 PL peak intensity in the PL spectrum of bundles of nanofibers requires a vanishing correlation length (l_0 = 0). The relaxed emitting exciton in bundles is thus localized on approximately 2.9 CBT cores due to the rough excited-state energy landscape along nanofibers in bundles (Figure 3F). The different excited-state energy landscapes along one column (single nanofiber and within a bundle, respectively) due to the distinct spatial transition energy correlations is visualized in Figure 3E,F. We note that these realizations are directly taken from the numerical simulations.

Direct Visualization of Exciton Transport. Our optical spectroscopy data demonstrate that we are able to tune the

https://dx.doi.org/10.1021/jacs.0c01392
J. Am. Chem. Soc. 2020, 142, 8323−8330

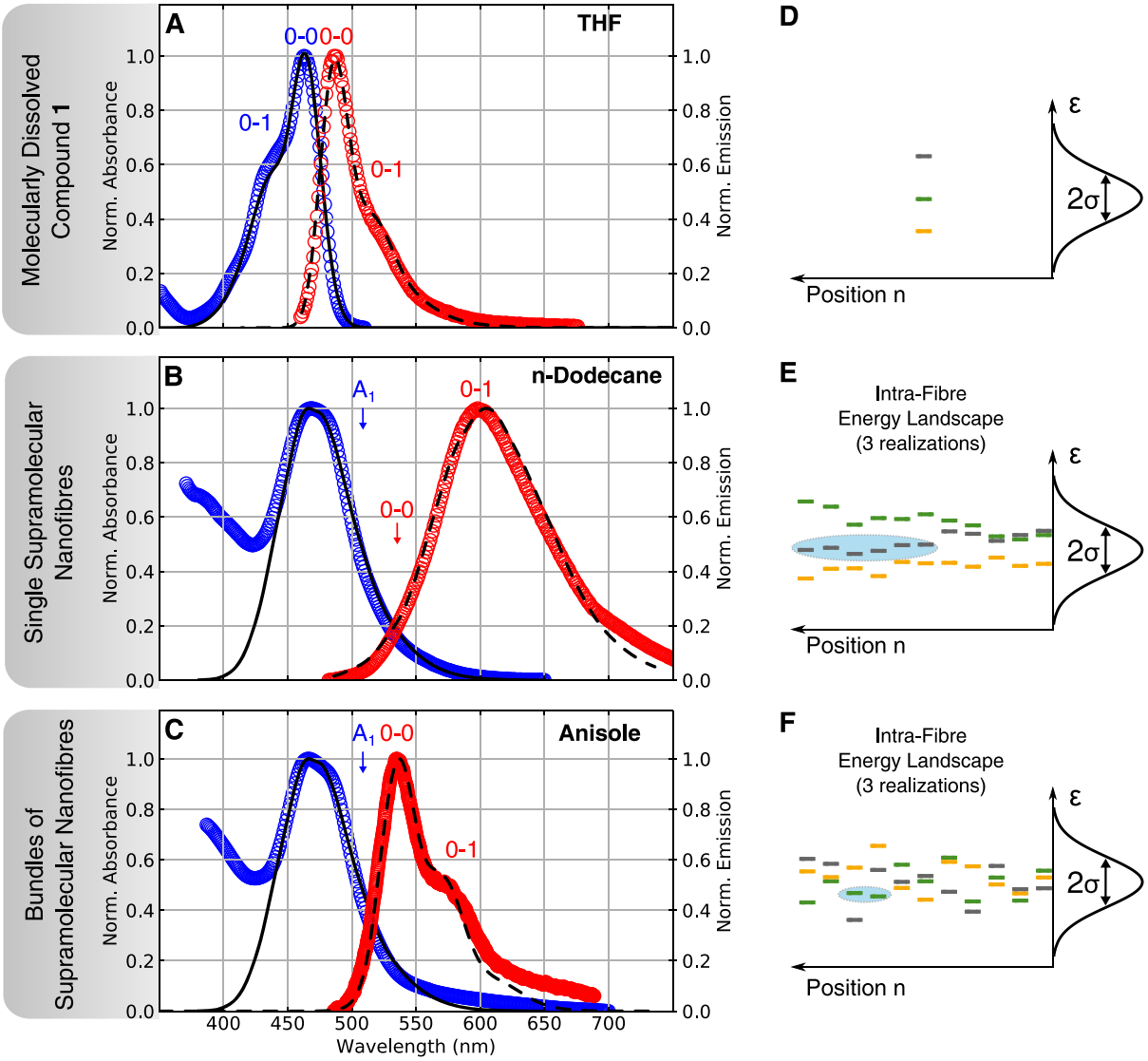

Figure 3. Optical properties of compound **1** and supramolecular architectures. (A) Normalized absorption (blue) and photoluminescence spectra (red) of dissolved compound **1** in THF (40 μM) with the corresponding Franck–Condon analysis (black lines). (B, C) Normalized absorption (blue) and photoluminescence spectra (red) of single supramolecular nanofibers in *n*-dodecane (40 μM) (B) and bundles of supramolecular nanofibers in anisole (200 μM) (C), together with simulated spectra based on a Frenkel–Holstein Hamiltonian (black lines). (D) Illustration of the inhomogeneous distribution of transition energies of dissolved compound **1** for three realizations. (E, F) Representation of three simulated realizations of transition energies of the building block at position n within one single column for the simulated spectra in B and C. The spatial correlation length of transition energies for single nanofibers is $l_0 \geq 10$ and for bundles of nanofibers $l_0 = 0$ (left, intracolumn energy landscape), while the corresponding ensemble averages, with a Gaussian width σ, over all columns (right) are almost identical. The ellipses indicate the delocalization of relaxed emitting states.

coherence characteristics of the relaxed excitons along the H-type columns by altering the hierarchical level of our architectures. These relaxed excitons are responsible for incoherent long-range transport, since they perform many hopping steps within their substantial excited-state lifetime in our H-aggregates. Importantly, the hopping rates of delocalized excitons have to be described by a generalized Förster theory, in which optically dark exciton states contribute to the hopping rates.[36−38] These systems are thus ideal to resolve the interplay between morphology, correlated electronic disorder, and coherence (delocalization) in the long-range incoherent transport of excitons along individual, spatially isolated nanostructures on pico- to nanosecond time scales. Figure 4A and B display representative wide-field PL images of isolated nanostructures, both with lengths of several micrometers, in agreement with the AFM data (Figure 2A,E). The single nanofiber shows a small PL signal (Figure 4A), which demonstrates the weakly optically allowed nature of the emitting excitons and thus the high degree of coherence within the nanofiber. The signal from the bundle of nanofibers is significantly stronger mainly owing to the large number of columns within the bundle (Figure 4B) and to a lesser extent due to the higher PL quantum efficiency of one column in a bundle (see Table S2).

Having located isolated nanostructures, we switched the microscope to confocal illumination and centered each nanostructure in the diffraction-limited focus of a pulsed laser (red dashed circles, Figure 4A,B). Combining detection-beam scanning with time-correlated single-photon counting[39] (see Supporting Information sections 1 and 6), we measured

https://dx.doi.org/10.1021/jacs.0c01392
J. Am. Chem. Soc. 2020, 142, 8323−8330

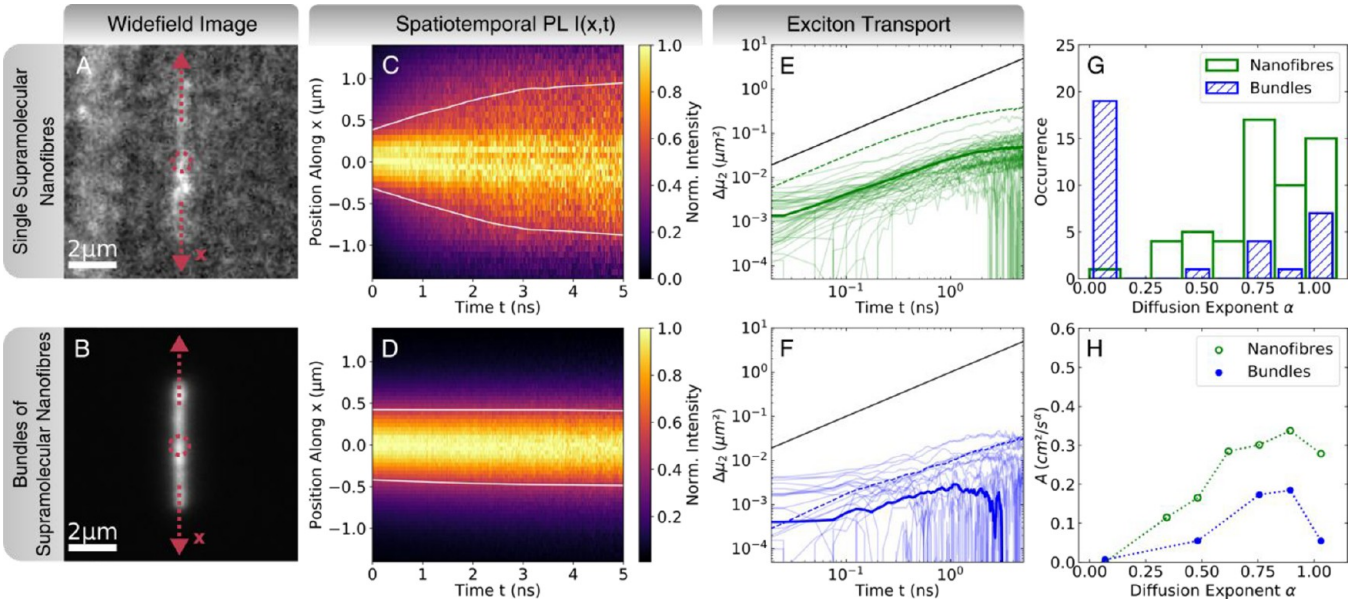

Figure 4. Direct visualization of long-range energy transport along supramolecular architectures. (A, B) Wide-field photoluminescence image of a single supramolecular nanofiber and a bundle of supramolecular nanofibers, respectively. Red dashed arrows indicate the scanning axis x; dashed circles label the position $x = 0$ of the excitation spot. (C, D) Normalized PL intensity distributions and their evolution in space and time for the single nanofiber in A and the bundle in B. The white contour lines indicate the time evolution of the full width at half-maximum. (E, F) Temporal changes of the second moments of the spatial intensity profiles for 56 nanofibers and 32 bundles of nanofibers (thin green and blue solid lines). The thick lines represent the average of all curves, and the dashed lines the evolution of the second moment for the data in C and D. The black lines indicate a linear scaling in time, i.e., normal diffusion, as a guide for the eye. (G) Distribution of the diffusion exponent α for all nanofibers (green) and bundles (blue) in E and F, evaluated for $t < 1$ ns. (H) Averaged hopping coefficients A as a function of α for nanofibers (green) and bundles (blue).

PL decay curves while scanning the detection position along the long axis of the nanostructures (dashed arrows in Figure 4A,B). Figure 4C and D show the resulting PL intensity distributions, $I(x, t)$, as a function of the distance x relative to the center of the excitation spot and time t after laser excitation. Normalization of the spatial intensity distributions at each point in time (Figure S13) reveals the broadening of the PL signal along the nanostructures' long axes on (sub-) nanosecond time scales. Hence, the initial singlet exciton population, created by the diffraction-limited excitation pulse, is transported away from the excitation spot prior to (radiative) decay. This energy transport is significantly more pronounced for the single nanofiber compared to the bundle of nanofibers (Figure 4C,D, white contour lines). We attribute this difference to the distinct excited-state energy landscapes (Figure 3E,F). We rule out artifacts due to saturation and technical issues, since we operate under very low excitation fluences, and we have performed an independent control experiment on a system that does not show long-range energy transport (see Supporting Information, Materials and Methods, and Figure S12).

To quantitatively describe the time-dependent broadening of the spatial intensity distributions, we calculated the second moments $\mu_2(t)$[22] at time t as a measure for their widths (Figure S13). We evaluated changes of $\mu_2(t)$ with respect to the second moment (width) of the initial distribution $\mu_2(0)$:

$$\Delta\mu_2(t) = \mu_2(t) - \mu_2(0) \tag{1}$$

The $\Delta\mu_2(t)$ curves retrieved from the data in Figure 4C,D are shown as thick dashed lines in Figure 4E,F. At short times ($t \leq 1$ ns), we find similar slopes for both curves. However, the $\Delta\mu_2(t)$ values for the single nanofiber are larger by more than 1 order of magnitude compared to those for the bundle. This observation reflects the faster and more pronounced broadening of the initial exciton population in the single nanofiber due to more efficient energy transport. For longer times ($t \geq 2.5$ ns) the broadening slows down and a plateau is reached for both architectures. We confirmed the same trend for in total 56 single nanofibers and 32 bundles, illustrated with thin solid green and blue lines in Figure 4E,F.

The second moments $\Delta\mu_2(t)$ follow to a good approximation a power law for $t < 1$ ns. We can thus fit the transport dynamics with a diffusion model[11,17,22,39−41] (see Supporting Information section 7):

$$\Delta\mu_2(t) = At^{\alpha} \tag{2}$$

Here α is the diffusion exponent and A is the exciton hopping coefficient, which is related to the time-dependent diffusivity $D(t) = \frac{1}{2}A_{\alpha}t^{\alpha-1}$. Figure 4G shows the exponents for nanofibers (green bars) and bundles (blue hatched bars) for all curves in Figure 4E,F. We find a broad distribution with $0 \leq \alpha \leq 1$ (for $t < 1$ ns) due to the intrinsic electronic disorder in deposited supramolecular nanostructures. For single nanofibers the mean exponent is $\bar{\alpha}_{\text{Fiber}} = 0.78 \pm 0.24$, and a significant fraction exhibits $\alpha \approx 1$, which indicates normal diffusion visualized in Figure 4E,F with black solid lines. In contrast, the mean exponent for bundles is smaller with $\bar{\alpha}_{\text{Fiber}} = 0.37 \pm 0.47$, which is characteristic for strongly subdiffusive transport due to the disordered energy landscape.[22] Notably, for bundles the highest occurrence of exponents is at $\alpha \approx 0$. This behavior is expected for a system with strong local electronic perturbations (Figure 3F), in which trapping hinders exciton transport.[22] For the single nanofibers the average exciton hopping coefficients A as a function of the exponent α are larger (Figure 4H). This

https://dx.doi.org/10.1021/jacs.0c01392
J. Am. Chem. Soc. 2020, 142, 8323−8330

translates into higher diffusivities $D(t)$ for single nanofibers: For example, for the nanofiber shown in Figure 4C we find $D_{Fiber}(t = 1\ ns) = 1.03\ cm^2/s$, which is the largest value reported for an H-aggregate and is more than 1 order of magnitude larger than the diffusivity for the bundle shown in Figure 4D with D_{Bundle} ($t = 1$ ns) = 0.05 cm^2/s (see also Figure S14).

CONCLUSION

Our H-type supramolecular architectures with different hierarchical levels represent a versatile system to understand the subtle interplay between electronic coupling, disorder, and coherence for efficient long-range, incoherent transport of delocalized singlet excitons. We have demonstrated remarkable differences in the spectroscopic properties as well as in the energy transport characteristics of single supramolecular nanofibers and bundles of nanofibers. The transition energies of adjacent CBT cores in single supramolecular nanofibers are spatially correlated, resulting in smooth excited-state energy landscapes. The concomitant high degree of coherence (exciton delocalization) facilitates long-range incoherent energy transport. In contrast, in bundles of nanofibers spatial correlations in the transition energies are found to be absent. This gives rise to a disordered excited-state energy landscape with strongly localized excitons. Hence, exciton transport is hindered by trapping in local energy minima.[22] The uncorrelated transition energies in bundles of nanofibers can be explained by very subtle local electronic perturbations due to interacting peripheries.[30] Alternatively, disorder on a local scale between columns may arise from a geometric frustration in a hexagonal packing due to compensation of macrodipoles.[42] Both effects can destroy shared electronic environments. Our observations are a manifestation of coherence-enhanced diffusivities of excitons[15,18,43] and highlight the critical role of spatially correlated transition energies of the supramolecular building blocks for long-range energy transport.[44] The present data therefore add a new dimension to the development of a detailed theoretical understanding of energy transport in columnar H-type supramolecular nanostructures[45] as well as for the design of novel, optimized nanophotonic applications.

ASSOCIATED CONTENT

Supporting Information

The Supporting Information is available free of charge at https://pubs.acs.org/doi/10.1021/jacs.0c01392.

Materials and methods; additional characterization of supramolecular architectures by AFM, electron diffraction, and optical spectroscopy; numerical simulations of optical spectra and exciton diffusion model (PDF)

AUTHOR INFORMATION

Corresponding Authors

Hans-Werner Schmidt − *Macromolecular Chemistry and Bavarian Polymer Institute, University of Bayreuth, 95447 Bayreuth, Germany;* orcid.org/0000-0002-1761-1153; Email: hans-werner.schmidt@uni-bayreuth.de

Richard Hildner − *Spectroscopy of Soft Matter, University of Bayreuth, 95447 Bayreuth, Germany; Zernike Institute for Advanced Materials, University of Groningen, 9747 AG Groningen, The Netherlands;* orcid.org/0000-0002-7282-3730; Email: r.m.hildner@rug.nl

Authors

Bernd Wittmann − *Spectroscopy of Soft Matter, University of Bayreuth, 95447 Bayreuth, Germany*

Felix A. Wenzel − *Macromolecular Chemistry and Bavarian Polymer Institute, University of Bayreuth, 95447 Bayreuth, Germany; Institute for Complex Molecular Systems, Laboratory of Macromolecular and Organic Chemistry, Eindhoven University of Technology, 5612, AZ, Eindhoven, The Netherlands*

Stephan Wiesneth − *Spectroscopy of Soft Matter, University of Bayreuth, 95447 Bayreuth, Germany*

Andreas T. Haedler − *Macromolecular Chemistry and Bavarian Polymer Institute, University of Bayreuth, 95447 Bayreuth, Germany; Institute for Complex Molecular Systems, Laboratory of Macromolecular and Organic Chemistry, Eindhoven University of Technology, 5612, AZ, Eindhoven, The Netherlands*

Markus Drechsler − *Bavarian Polymer Institute, University of Bayreuth, 95447 Bayreuth, Germany*

Klaus Kreger − *Macromolecular Chemistry and Bavarian Polymer Institute, University of Bayreuth, 95447 Bayreuth, Germany;* orcid.org/0000-0003-3021-1311

Jürgen Köhler − *Spectroscopy of Soft Matter, University of Bayreuth, 95447 Bayreuth, Germany;* orcid.org/0000-0002-4214-4008

E. W. Meijer − *Institute for Complex Molecular Systems, Laboratory of Macromolecular and Organic Chemistry, Eindhoven University of Technology, 5612, AZ, Eindhoven, The Netherlands;* orcid.org/0000-0003-4126-7492

Complete contact information is available at: https://pubs.acs.org/10.1021/jacs.0c01392

Notes

The authors declare no competing financial interest.

ACKNOWLEDGMENTS

We acknowledge financial support from the German Research Foundation (DFG) through the research training group GRK1640 and from the Bavarian State Ministry of Science and the Arts through the Collaborative Research Network "Solar Technologies go Hybrid". We acknowledge support by the Elite Network of Bavaria (ENB) through the study programs "Macromolecular Science" (F.A.W.) and "Biological Physics" (R.H.) as well as the Max-Weber program (F.A.W.). We are grateful to Doris Hanft and Sandra Ganzleben (Macromolecular Chemistry, University of Bayreuth) for their help with syntheses. We thank Markus Hund (KeyLab Surface and Interface Characterization) of the Bavarian Polymer Institute for support with AFM measurements and Sooruban Shanmugaratnam (Biochemistry, University of Bayreuth) for help with CD spectroscopy.

REFERENCES

(1) Sengupta, S.; Würthner, F. Chlorophyll J-Aggregates: From Bioinspired Dye Stacks to Nanotubes, Liquid Crystals, and Biosupramolecular Electronics. *Acc. Chem. Res.* **2013**, *46* (11), 2498−2512.

(2) Liess, A.; Arjona-Esteban, A.; Kudzus, A.; Albert, J.; Krause, A. M.; Lv, A.; Stolte, M.; Meerholz, K.; Würthner, F. Ultranarrow Bandwidth Organic Photodiodes by Exchange Narrowing in Merocyanine H- and J-Aggregate Excitonic Systems. *Adv. Funct. Mater.* **2019**, *29* (21), 1−9.

(3) Aida, T.; Meijer, E. W.; Stupp, S. I. Functional Supramolecular Polymers. *Science* **2012**, *335* (6070), 813−817.
(4) Boulais, E.; Sawaya, N. P. D.; Veneziano, R.; Andreoni, A.; Banal, J. L.; Kondo, T.; Mandal, S.; Lin, S.; Schlau-Cohen, G. S.; Woodbury, N. W.; Yan, H.; Aspuru-Guzik, A.; Bathe, M. Programmed Coherent Coupling in a Synthetic DNA-Based Excitonic Circuit. *Nat. Mater.* **2018**, *17* (2), 159−166.
(5) Moulin, E.; Armao, J. J.; Giuseppone, N. Triarylamine-Based Supramolecular Polymers: Structures, Dynamics, and Functions. *Acc. Chem. Res.* **2019**, *52* (4), 975−983.
(6) Korevaar, P. A.; George, S. J.; Markvoort, A. J.; Smulders, M. M. J.; Hilbers, P. A. J.; Schenning, A. P. H. J.; De Greef, T. F. A.; Meijer, E. W. Pathway Complexity in Supramolecular Polymerization. *Nature* **2012**, *481* (7382), 492−496.
(7) Ciesielski, A.; Palma, C.-A.; Bonini, M.; Samori, P. Towards Supramolecular Engineering of Functional Nanomaterials: Pre-Programming Multi-Component 2D Self-Assembly at Solid-Liquid Interfaces. *Adv. Mater.* **2010**, *22*, 3506−3520.
(8) Scholes, G. D.; Fleming, G. R.; Chen, L. X.; Aspuru-Guzik, A.; Buchleitner, A.; Coker, D. F.; Engel, G. S.; Van Grondelle, R.; Ishizaki, A.; Jonas, D. M.; Lundeen, J. S.; McCusker, J. K.; Mukamel, S.; Ogilvie, J. P.; Olaya-Castro, A.; Ratner, M. A.; Spano, F. C.; Whaley, K. B.; Zhu, X. Using Coherence to Enhance Function in Chemical and Biophysical Systems. *Nature* **2017**, *543* (7647), 647−656.
(9) Jin, X. H.; Price, M. B.; Finnegan, J. R.; Boott, C. E.; Richter, J. M.; Rao, A.; Matthew Menke, S.; Friend, R. H.; Whittell, G. R.; Manners, I. Long-Range Exciton Transport in Conjugated Polymer Nanofibers Prepared by Seeded Growth. *Science* **2018**, *360* (6391), 897−900.
(10) Winiger, C. B.; Li, S.; Kumar, G. R.; Langenegger, S. M.; Häner, R. Long-Distance Electronic Energy Transfer in Light-Harvesting Supramolecular Polymers. *Angew. Chem., Int. Ed.* **2014**, *53* (49), 13609−13613.
(11) Clark, K. A.; Krueger, E. L.; Vanden Bout, D. A. Direct Measurement of Energy Migration in Supramolecular Carbocyanine Dye Nanotubes. *J. Phys. Chem. Lett.* **2014**, *5* (13), 2274−2282.
(12) Caram, J. R.; Doria, S.; Eisele, D. M.; Freyria, F. S.; Sinclair, T. S.; Rebentrost, P.; Lloyd, S.; Bawendi, M. G. Room-Temperature Micron-Scale Exciton Migration in a Stabilized Emissive Molecular Aggregate. *Nano Lett.* **2016**, *16* (11), 6808−6815.
(13) Lin, H.; Camacho, R.; Tian, Y.; Kaiser, T. E.; Würthner, F.; Scheblykin, I. G. Collective Fluorescence Blinking in Linear J-Aggregates Assisted by Long-Distance Exciton Migration. *Nano Lett.* **2010**, *10* (2), 620−626.
(14) Wan, Y.; Stradomska, A.; Knoester, J.; Huang, L. Direct Imaging of Exciton Transport in Tubular Porphyrin Aggregates by Ultrafast Microscopy. *J. Am. Chem. Soc.* **2017**, *139* (21), 7287−7293.
(15) Brédas, J. L.; Sargent, E. H.; Scholes, G. D. Photovoltaic Concepts Inspired by Coherence Effects in Photosynthetic Systems. *Nat. Mater.* **2017**, *16* (1), 35−44.
(16) Fassioli, F.; Dinshaw, R.; Arpin, P. C.; Scholes, G. D. Photosynthetic Light Harvesting: Excitons and Coherence. *J. R. Soc., Interface* **2014**, *11* (92), 20130901.
(17) Menke, S. M.; Holmes, R. J. Exciton Diffusion in Organic Photovoltaic Cells. *Energy Environ. Sci.* **2014**, *7* (2), 499−512.
(18) Scholes, G. D. Designing Light-Harvesting Antenna Systems Based on Superradiant Molecular Aggregates. *Chem. Phys.* **2002**, *275* (1−3), 373−386.
(19) Topczak, A. K.; Roller, T.; Engels, B.; Brütting, W.; Pflaum, J. Nonthermally Activated Exciton Transport in Crystalline Organic Semiconductor Thin Films. *Phys. Rev. B: Condens. Matter Mater. Phys.* **2014**, *89* (20), 201203.
(20) Sung, J.; Kim, P.; Fimmel, B.; Würthner, F.; Kim, D. Direct Observation of Ultrafast Coherent Exciton Dynamics in Helical π-Stacks of Self-Assembled Perylene Bisimides. *Nat. Commun.* **2015**, *6* (1), 8646.
(21) Moix, J. M.; Khasin, M.; Cao, J. Coherent Quantum Transport in Disordered Systems: I. the Influence of Dephasing on the Transport Properties and Absorption Spectra on One-Dimensional Systems. *New J. Phys.* **2013**, *15* (8), 085010.
(22) Vlaming, S. M.; Malyshev, V. A.; Eisfeld, A.; Knoester, J. Subdiffusive Exciton Motion in Systems with Heavy-Tailed Disorder. *J. Chem. Phys.* **2013**, *138* (21), 214316.
(23) Haedler, A. T.; Kreger, K.; Issac, A.; Wittmann, B.; Kivala, M.; Hammer, N.; Köhler, J.; Schmidt, H. W.; Hildner, R. Long-Range Energy Transport in Single Supramolecular Nanofibres at Room Temperature. *Nature* **2015**, *523* (7559), 196−199.
(24) Spano, F. C.; Clark, J.; Silva, C.; Friend, R. H. Determining Exciton Coherence from the Photoluminescence Spectral Line Shape in Poly(3-Hexylthiophene) Thin Films. *J. Chem. Phys.* **2009**, *130* (7), 074904.
(25) Mohseni, M.; Aspuru-Guzik, A.; Rebentrost, P.; Shabani, A.; Lloyd, S.; Huelga, S. F.; Plenio, M. B. Environment-Assisted Quantum Transport. In *Quantum Effects in Biology*; Cambridge University Press, 2014; pp 159−176.
(26) Novo, L.; Mohseni, M.; Omar, Y. Disorder-Assisted Quantum Transport in Suboptimal Decoherence Regimes. *Sci. Rep.* **2016**, *6* (1), 18142.
(27) Fukui, T.; Kawai, S.; Fujinuma, S.; Matsushita, Y.; Yasuda, T.; Sakurai, T.; Seki, S.; Takeuchi, M.; Sugiyasu, K. Control over Differentiation of a Metastable Supramolecular Assembly in One and Two Dimensions. *Nat. Chem.* **2017**, *9* (5), 493−499.
(28) Wagner, W.; Wehner, M.; Stepanenko, V.; Würthner, F. Supramolecular Block Copolymers by Seeded Living Polymerization of Perylene Bisimides. *J. Am. Chem. Soc.* **2019**, *141* (30), 12044−12054.
(29) Eisele, D. M.; Arias, D. H.; Fu, X.; Bloemsma, E. A.; Steiner, C. P.; Jensen, R. A.; Rebentrost, P.; Eisele, H.; Tokmakoff, A.; Lloyd, S.; Nelson, K. A.; Nicastro, D.; Knoester, J.; Bawendi, M. G. Robust Excitons Inhabit Soft Supramolecular Nanotubes. *Proc. Natl. Acad. Sci. U. S. A.* **2014**, *111* (33), E3367−E3375.
(30) Kim, T.; Ham, S.; Lee, S. H.; Hong, Y.; Kim, D. Enhancement of Exciton Transport in Porphyrin Aggregate Nanostructures by Controlling the Hierarchical Self-Assembly. *Nanoscale* **2018**, *10* (35), 16438−16446.
(31) Marty, R.; Szilluweit, R.; Sánchez-Ferrer, A.; Bolisetty, S.; Adamcik, J.; Mezzenga, R.; Spitzner, E.-C.; Feifer, M.; Steinmann, S. N.; Corminboeuf, C.; Frauenrath, H. Hierarchically Structured Microfibers of "Single Stack" Perylene Bisimide and Quaterthiophene Nanowires. *ACS Nano* **2013**, *7* (10), 8498−8508.
(32) Haedler, A. T.; Meskers, S. C. J.; Zha, R. H.; Kivala, M.; Schmidt, H. W.; Meijer, E. W. Pathway Complexity in the Enantioselective Self-Assembly of Functional Carbonyl-Bridged Triarylamine Trisamides. *J. Am. Chem. Soc.* **2016**, *138* (33), 10539−10545.
(33) Valera, J. S.; Gómez, R.; Sánchez, L. Tunable Energy Landscapes to Control Pathway Complexity in Self-Assembled N-Heterotriangulenes: Living and Seeded Supramolecular Polymerization. *Small* **2018**, *14* (3), 1702437.
(34) Haedler, A. T.; Beyer, S. R.; Hammer, N.; Hildner, R.; Kivala, M.; Köhler, J.; Schmidt, H. W. Synthesis and Photophysical Properties of Multichromophoric Carbonyl-Bridged Triarylamines. *Chem. - Eur. J.* **2014**, *20* (37), 11708−11718.
(35) Hestand, N. J.; Spano, F. C. Expanded Theory of H- and J-Molecular Aggregates: The Effects of Vibronic Coupling and Intermolecular Charge Transfer. *Chem. Rev.* **2018**, *118* (15), 7069−7163.
(36) Sumi, H. Bacterial Photosynthesis Begins with Quantum-Mechanical Coherence. *Chem. Rec.* **2001**, *1* (6), 480−493.
(37) Scholes, G. D.; Jordanides, X. J.; Fleming, G. R. Adapting the Förster Theory of Energy Transfer for Modeling Dynamics in Aggregated Molecular Assemblies. *J. Phys. Chem. B* **2001**, *105* (8), 1640−1651.
(38) Beljonne, D.; Curutchet, C.; Scholes, G. D.; Silbey, R. J. Beyond Förster Resonance Energy Transfer in Biological and Nanoscale Systems. *J. Phys. Chem. B* **2009**, *113* (19), 6583−6599.

https://dx.doi.org/10.1021/jacs.0c01392
J. Am. Chem. Soc. 2020, 142, 8323−8330

(39) Akselrod, G. M.; Deotare, P. B.; Thompson, N. J.; Lee, J.; Tisdale, W. A.; Baldo, M. A.; Menon, V. M.; Bulovic, V. Visualization of Exciton Transport in Ordered and Disordered Molecular Solids. *Nat. Commun.* **2014**, *5* (1), 3646.
(40) Havlin, S.; Ben-Avraham, D. Diffusion in Disordered Media. *Adv. Phys.* **2002**, *51* (1), 187−292.
(41) Wu, J.; Berland, K. M. Propagators and Time-Dependent Diffusion Coefficients for Anomalous Diffusion. *Biophys. J.* **2008**, *95* (4), 2049−2052.
(42) Zehe, C. S.; Hill, J. A.; Funnell, N. P.; Kreger, K.; van der Zwan, K. P.; Goodwin, A. L.; Schmidt, H.-W.; Senker, J. Mesoscale Polarization by Geometric Frustration in Columnar Supramolecular Crystals. *Angew. Chem., Int. Ed.* **2017**, *56* (16), 4432−4437.
(43) Lloyd, S.; Mohseni, M. Symmetry-Enhanced Supertransfer of Delocalized Quantum States. *New J. Phys.* **2010**, *12* (7), 075020.
(44) Lee, C. K.; Shi, L.; Willard, A. P. Modeling the Influence of Correlated Molecular Disorder on the Dynamics of Excitons in Organic Molecular Semiconductors. *J. Phys. Chem. C* **2019**, *123* (1), 306−314.
(45) Saikin, S. K.; Shakirov, M. A.; Kreisbeck, C.; Peskin, U.; Proshin, Y. N.; Aspuru-Guzik, A. On the Long-Range Exciton Transport in Molecular Systems: The Application to H-Aggregated Heterotriangulene Chains. *J. Phys. Chem. C* **2017**, *121* (45), 24994−25002.

https://dx.doi.org/10.1021/jacs.0c01392
J. Am. Chem. Soc. 2020, 142, 8323−8330